Fibers and Polymers (2023) 24:959–973
https://doi.org/10.1007/s12221-023-00030-0

Online ISSN 1875-0052
Print ISSN 1229-9197

REGULAR ARTICLE

Bactericidal Properties of Natural Fibers Hybrid Functionalized with ZnO/Cu^{2+} and ZnO/Cu^{0}

Daniel J. da Silva[1] · Alana G. Souza[1] · Paulo H. Camani[1] · Derval S. Rosa[1]

Received: 17 January 2022 / Revised: 19 March 2022 / Accepted: 13 April 2022 / Published online: 22 February 2023

Abstract

Multifunctional natural fibers with antimicrobial properties have been applied as a viable strategy to prevent microorganism contamination and proliferation on the surface of clothes and personal protection equipment marketed and used by health professionals, patients, and the general population. They present intrinsic antimicrobial capacity, providing effective protection preventing the transmission and contagion of diseases caused by pathogenic microorganisms. Herein, we successfully functionalized cotton fibers with ZnO/Cu^{2+} and ZnO/Cu^{0} hybrid systems via a hydrothermal routine. Rietveld refinement from X-ray Diffractometry (XRD) data and Fourier-Transform Raman Spectroscopy (FT-Raman) indicate alterations on the cellulose crystallinity index in the cotton fibers after functionalization, mainly on the proportion of cellulose I_{β} polymorph crystal. Scanning Electron Microscopy (SEM) and X-ray photoelectron spectroscopy (XPS) indicate adequate ZnO nanoparticles fixation and in-situ reduction of copper ions. Antimicrobial tests confirm that the multifunctional fibers present bactericidal activity against Gram-negative and Gram-positive bacteria under electromagnetic irradiation (440–480 nm). Self-disinfection capability and UV blocking properties of wipes with fibers after ZnO/Cu^{2+} and ZnO/Cu^{0} functionalization were improved.

Graphical abstract

Keywords Cellulose biopolymer · Functionalization · Morphology · Natural fibers · Multifunctional textiles

✉ Derval S. Rosa
dervalrosa@yahoo.com.br

[1] Center for Engineering, Modeling, and Applied Social Sciences (CECS), Federal University of ABC (UFABC), Av. Dos Estados, 5001. CEP, Santo André, SP 09210-210, Brazil

1 Introduction

Synthetic fibers of polypropylene, polyesters, and polyamides are currently the major components used in the textile industry for clothing and body protective equipment,

displaying an essential role in the quality and preservation of human life. However, these synthetic polymers promote several issues associated with waste generation leading to environmental impacts with potentially harmful effects to the health of living organisms on the Earth [1–4]. Consequently, natural fibers have been drawing attention due to the biodegradability that is less dangerous to the environment when discarded after their end-use application [5, 6].

Cotton is a biomaterial from the removable biomass that is applied to manufacture low-cost textiles without the need for animal exploitation [7]. Moreover, natural fibers from cotton are suitable for producing fabrics with wearability and breathability, good for making wearer-friendly clothing [8]. However, cotton fibers present suitable features to support the proliferation of microorganisms (bacteria and fungi) on their surfaces [9], which can reduce the fabric lifetime and bring on potential risks to human health [10]. After the COVID-19 pandemic occasioned by the severe acute respiratory syndrome coronavirus 2 (SARS-CoV-2), the textile industry has been seeking to develop multifunctional fibers with antimicrobial properties to prevent the virus transmission and guarantee more effective protection of the people that is crucial in hospitals, medical clinics, and health centers. Also, SARS-CoV-2 maintains its potential for transmission and infection on the conventional materials' surfaces even after 24 h [11]. Therefore, antimicrobial fibers with capacity for self-disinfection is fundamental to prevent these epidemiologic issues.

Nanotechnology has been focused on the development of new multifunctional fibers that, in addition to presenting antimicrobial activity, have other advanced functional properties, such as ultraviolet protection, anti-odor, water repellency, electrical conductivity, and self-cleaning [12, 13], without the loss of softness, flexibility, and washability required by the users.

Metals and oxides can provide self-disinfecting properties for developing antimicrobial fibers [14, 15]. Silver (Ag), gold (Au), platinum (Pt), copper (Cu), zinc oxide (ZnO), copper oxide II (CuO), silicon dioxide (SiO_2), and titanium dioxide (TiO_2) are recognized by their intrinsic antimicrobial activities and being technologically feasible for this purpose [16–19]. Their bactericidal and fungicidal properties involve generating reactive oxygen species (ROS) that destroy lipids, DNA, RNA, and proteins. Also, the bacteria reproducing cycle is interrupted by metal ions' release since the metal ion aggregation in amines and phosphates chemical groups cause irreversible damage to essential biomolecules for the cells (proteins, phospholipids, and nucleic acids) [14, 15, 18]. For these reasons, silver and other intrinsic antimicrobial disinfectants, such as citric acid, have been suggested to be used as disinfectants agents against SARS-CoV-2 by the United States Environmental Protection Agency (USEPA) even though they have not been directly tested with this coronavirus and its strains [20].

Different methodologies have been utilized to synthesize *in-situ* oxide and metal antimicrobial nanoparticles onto the surface of cotton fibers, such as hydrothermal [12, 21–25], sono-chemical route [8, 26], microwave-assisted synthesis [27], exhaustion bath [28–31], and plasma treatment [3, 32]. To avoid environmental impacts, the in situ synthesis of these nanoparticles by hydrothermal route can be conducted using reagents with lower toxicity, such as citric acid and ascorbic acid [23, 33, 34].

In this contribution, we successfully functionalized cotton fibers with ZnO and copper via the hydrothermal procedure. The functionalized fibers were evaluated by several techniques, such as X-ray Diffractometry (XRD), Fourier-Transform Raman Spectroscopy (FT-Raman), colorimetry, Scanning Electron Microscopy (SEM), uniaxial tensile tests, X-ray photoelectron spectroscopy (XPS), to understand the influence in their macroscopic, surface and morphological changes of the cotton fibers caused by the functionalization procedure using different citric acid content (reductant/binder agent). Also, the antimicrobial activity of wipes with the multifunctional fibers against Gram-negative (*Escherichia coli*, *E. coli*) and Gram-positive (*Staphylococcus aureus*, *S. aureus*) bacteria was investigated by agar diffusion and liquid growth inhibition tests. The bactericidal performance of the multifunctional wipes was significantly affected by lighting exposition.

2 Materials and Methods

2.1 Materials

The cotton textile was acquired from a fabric store (São Paulo, Brazil). ZnO particles were purchased from Sigma-Aldrich Inc. (São Paulo, Brazil). Labsynth Produtos para Laboratorios Ltda. (São Paulo, Brazil) supplied the neutral detergent, citric acid, and copper nitrate trihydrate.

2.2 Coating Procedures

The cotton wipes with a dimension of 20×20 cm were immersed in an aqueous detergent solution (6.7 g L^{-1}) for 30 min. Subsequently, they were washed and soaked in water (15 min). Then, the samples were gently squeezed and kept at 110 ± 5 °C until they were completely dried. The washed cotton wipes were named *CF*. After this prewashing step, the samples were immersed in 250 mL of a dispersion bath (zinc oxide, citric acid, and copper nitrate trihydrate) and heated in a water bath at 70 °C (30 min). The dispersion baths were made up of $Cu(NO_3)_2 \cdot 3H_2O$ (400 ppm of Cu^{2+}), zinc oxide (400 ppm), and citric acid (0, 1, 3, 5, and 10 g L^{-1}). Samples

were named Thermal-X, where *X* corresponds to the citric acid concentration in the hydrothermal approach.

Then, the cotton wipes were taken out, squeezed, washed with water, and dried at 120 ± 5 °C (15 min). The schematic representation of the coating methodologies is illustrated in Fig. 1.

2.3 Characterization

2.3.1 Scanning Electron Microscopy (SEM)

Cotton wipes (1 cm × 1 cm) were coated with a 25 nm thick gold layer, using Sputtering Leica EM ACE 200 (Leica Microsystems, Wetzlar, Germany). Micrographs were performed using a microscope FEI Quanta 250 (Thermo Fisher Scientific, Hillsboro, Oregon, USA), using an accelerating voltage of 10 kV and a spot size of 4.

2.3.2 Dynamic Light Scattering (DLS)

The hydrodynamic radius of the particles in the liquor bath was characterized by dynamic light scattering (DLS) technique, with a stable 90° scattering angle, using Zetasizer Nano-ZS (Malvern Panalytical Ltd., Malvern, UK). Aliquots of 100 µL were suspended in distilled water (2 mL).

2.3.3 X-ray Photoelectron Spectroscopy (XPS)

The XPS analysis was performed using K-alpha^{+} equipment (ThermoFisher Scientific Inc., Massachusetts, USA) with monochromatic radiation A1Kα at room temperature.

2.3.4 FT-Raman

The wipes were analyzed with an FT-Raman – MultiRaman, Bruker Optics (Massachusetts, EUA), equipped with a 1064 nm wavelength (power laser = 100 W). The data acquisition was carried out in a range of 400–4000 cm^{-1}, 32 scans, and with 4 cm^{-1} spectral resolutions.

2.3.5 X-Ray Diffractometry (XRD)

X-Ray diffractometry was performed using a D8 Focus X-ray Diffractometer (Bruker, Massachusetts, USA), using CuKα (λ = 1.54056 Å) radiation operating and transmission mode. XRD data were collected in the range of 10–80° at each 0.015° (counting time = 1.5 s).

Rietveld refinements were performed on software Profex 4.3.0 [35]. All parameters were refined by the least-squares method. The tripled pseudo-Voigt function was used to model the peak shapes. Instrumental resolution function parameters were obtained from the database of the software Profex, entitled *d8-solxe-vds-12 mm*. The background function was the Lagrangian polynomial of the nth order. The polynomial order was determined automatically by the software Profex, depending on the angular range.

The cellulose I_β and II monoclinic crystal structures reported by French [36] were used for Rietveld fitting. The atomic positions and atomic displacement parameters were refined. The Lorentzian function was applied to model the contribution of the pattern background from the amorphous cellulose phase. The relative proportions of cellulose I_β and II (CI_c) were determined by integration their respective XRD diffractograms calculated in the whole range 2θ (10–80°), using the Eq. (1).

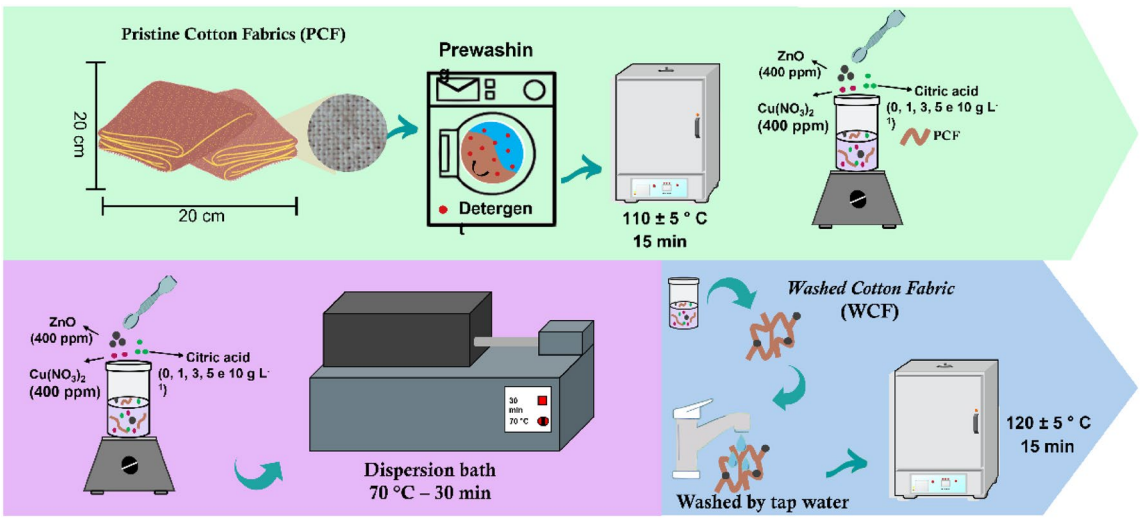

Fig. 1 Schematic representation of the adopted methodology

$$CI_c(\%) = 100 \times \frac{\int_{2\theta=10^\circ}^{2\theta=80^\circ} I_{cal-C} d(2\theta)}{\int_{2\theta=10^\circ}^{2\theta=80^\circ} I_{cal} d(2\theta) - \int_{2\theta=10^\circ}^{2\theta=80^\circ} I_{back} d(2\theta)} \quad (1)$$

where I_{back} and I_{cal-C} are the signal intensities of X-ray diffractogram calculated by Rietveld refinement from x-ray equipment background and cellulose crystals (cellulose I_β or II), in that order. I_{cal} is the total area of the X-ray diffractogram estimated by the refinement. The XRD crystallinity index (CI_{XRD}) corresponds to the total cellulose crystallinity (sum of the relative proportions of cellulose I_β and II).

2.3.6 Wetness

Moisture content (W) was measured by monitoring the weight of samples (0.5 × 0.5 cm) before and after drying at 105 °C for 2 h. moisture content was determined by Eq. (2)

$$W(\%) = 100 \times \frac{(M_i - M_f)}{M_i} \quad (2)$$

where M_i and M_j are the weight (g) of the sample before and after being dried, respectively. The wetness tests were conducted in triplicate.

2.3.7 UV–Visible Spectroscopy (UV–Vis Spectroscopy)

The transmission of ultraviolet (UV) and visible electromagnetic radiation through cotton wipes was assessed by a double-beam T80 UV–Visible spectrometer (PG Instruments Ltd) at the wavelength range 290–800 nm. The transmittance of UVB (290–315 nm), T(UVB), the transmittance of UVA (315–400 nm), T(UVA), and Ultraviolet Protection Factor (UPF) were determined according to Australian/New Zealand standard® AS/NZS 4399:1996.

2.3.8 Mechanical Properties

The samples were evaluated by uniaxial tensile testing (ABNT NBR ISO 13934), using universal tensile test equipment from Instron (USA), model 3367. The mechanical properties were measured by a uniaxial traction test (load cell of 50 N, and a test speed of 50 mm min^{-1}).

2.3.9 Colorimetry

The CIE Lab 1976's color coordinates (L*, a*, b*) for the samples were measured by a portable spectrophotometer (Spectro-Guide Sphere Gloss, BYK Gardner, USA), using 10° observer with D65 illuminant configuration and d/8 viewing geometry. L* corresponds to lightness from black (0) to white (100). a* and b* are the red(+)/green(−) and yellow(+)/blue(−) chromatic ratios, respectively [9, 36]. The average values of color coordinates were reported here from the measurements performed at three different regions of the samples. The total color difference (ΔE) was determined by Eq. (3) [37].

$$\Delta E = \left[(\Delta L^*)^2 + (\Delta a^*)^2 + (\Delta b^*)^2\right]^{0.5} \quad (3)$$

where ΔL, Δa, and Δb are the differences in the corresponding parameter value between samples with pristine fibers (CF) and with all functionalized fibers.

The whiteness index (WI) was calculated by Eq. (4) [38].

$$WI = 100 - \left[(100 - L^*)^2 + (a^*)^2 + (b^*)^2\right]^{0.5} \quad (4)$$

2.3.10 Antimicrobial Tests

The antimicrobial test was performed by a liquid growth inhibition test against *Staphylococcus aureus* (*S. aureus*, ATCC 6548) and *Escherichia coli* (*E. coli*, ATCC 25,922), as reported in the literature [39]. The multifunctional wipes were cut in squares (1 cm × 1 cm) and were added to a test tube containing a nutrient culture medium (Mueller–Hilton agar, Oxoid) with the bacteria (final count of 10^5 UFC mL^{-1}). The test tubes were kept for 24 h (without illumination) and 48 h (under lightning of a blue-emitting lamp of 150 Watts) in a microbiological oven at 36 ± 1 °C. After incubation, the antibacterial activity (AAc) was estimated using the absorbance of the liquid growth medium at 600 nm using UV–Vis spectrometer (UV-M51 BEL, Monza MB, Italy) and Eq. (5).

$$AAc(\%) = 100 \times \left(\frac{A_o - A}{A_o}\right) \quad (5)$$

where A_o and A are the absorbances of the control and the sample at 600 nm, respectively.

The inhibition zone was determined by agar diffusion tests. In this way, the samples (1 cm × 1 cm) were placed in contact with the sterilized Petri dishes with nutrient agar culture medium, Mueller–Hinton agar (KASVI), and inoculated with *E. coli* bacteria suspension at 10^5 CFU mL^{-1}, which were incubated at 36 ± 1 °C and 85% humidity. The inoculums viability was confirmed via a spread-plate method on agar nutrient medium as the positive control. The inhibition zone from the biocidal activity of the samples was evaluated after 48 h of incubation, under and without lightning of a white fluorescent lamp (150 Watts).

2.3.11 Statistical Analysis

Two-way analysis of variance (ANOVA two-way) and Tukey's test were applied to statistically evaluate the significant

differences between the samples' measured properties, using the Origin program (version 2016) and a 95% confidence level.

3 Results and Discussion

3.1 Scanning Electron Microscopy (SEM)

The presence of microparticles on the surface of the functionalized cotton fibers was evidenced by the SEM images presented in Fig. 2. Figure 2a shows the surface morphology of the cotton fibers (CF sample) without roughness or other surficial defects on a micrometer scale. Ibrahim and co-workers also performed a surface modification of the cotton fibers and cotton/polyester blend. They observed a clean surface for raw cotton fiber [40], similar to Fig. 2a.

Figure. 2b–f presents SEM images of samples after the hydrothermal treatment, and all the samples had microparticles in their surfaces. These particles were not observed in the washed CF, thus proving the coating's efficiency of ZnO and copper particles on the treated cotton fiber surface [41]. Yazdanshenas and Shateri-Khalilabad [41] developed cotton fabrics from alkali treatment with NaOH, whose sodium hydroxide was used as a reductant agent to obtain silver nanoparticles on the cotton fiber surface. The silver nanoparticles were observed for treated natural fibers from SEM images due to strong ionic interaction between metallic ions and functional groups inserted on the fiber's surface [41].

Even without citric acid (reductant/binder agent) (Fig. 2b), few particles were observed on the fiber surface that corresponds to the presence of ZnO-NPs imprisoned in the cotton fibers as suggested by the signals of Zn at 1022.9 and 1044.1 eV on the Zn_{2p} XPS spectra (Fig. 1S), Supplementary information). The signals are slightly higher than 1020.7 (ZnO $2p_{3/2}$) and 1043.5 eV (ZnO $2p_{1/2}$) [12], indicating a specific interaction binding of the ZnO on the cotton fibers, probably Zn-OH–cellulose coordination on the cotton's surface. Moreover, the Cu_{2p} XPS spectra (Fig. 1S) evidence that the copper cations are not reduced to Cu^0 without citric acid, but they remain in the cotton fibers like $Cu(OH)_2$ even after washing the thermal-0% sample (binding signals at 936.2, $Cu(OH)_2$ $2p_{3/2}$, and 955.1, $Cu(OH)_2$ $2p_{1/2}$) [42]. Also, DLS data (Fig. 3a) confirm that CuNPs are not formed in the suspension bath of the thermal-0% sample.

Sadanand and co-workers verified the presence of silver nanoparticles on the fiber's surface due to the efficiency of the simple hydrothermal one-step treatment. They described that Ag-NPs coating occurred due to both acts of the hydroxyl and carboxyl groups of cotton fibers in reducing reaction [43]. Then, the OH groups of the cellulose in the cotton fibers cannot act as reducing points of copper cations using the hydrothermal procedure of this work.

With the addition of citric acid (samples thermal-1%, thermal-3%, thermal-5%, and thermal-10%), the number of

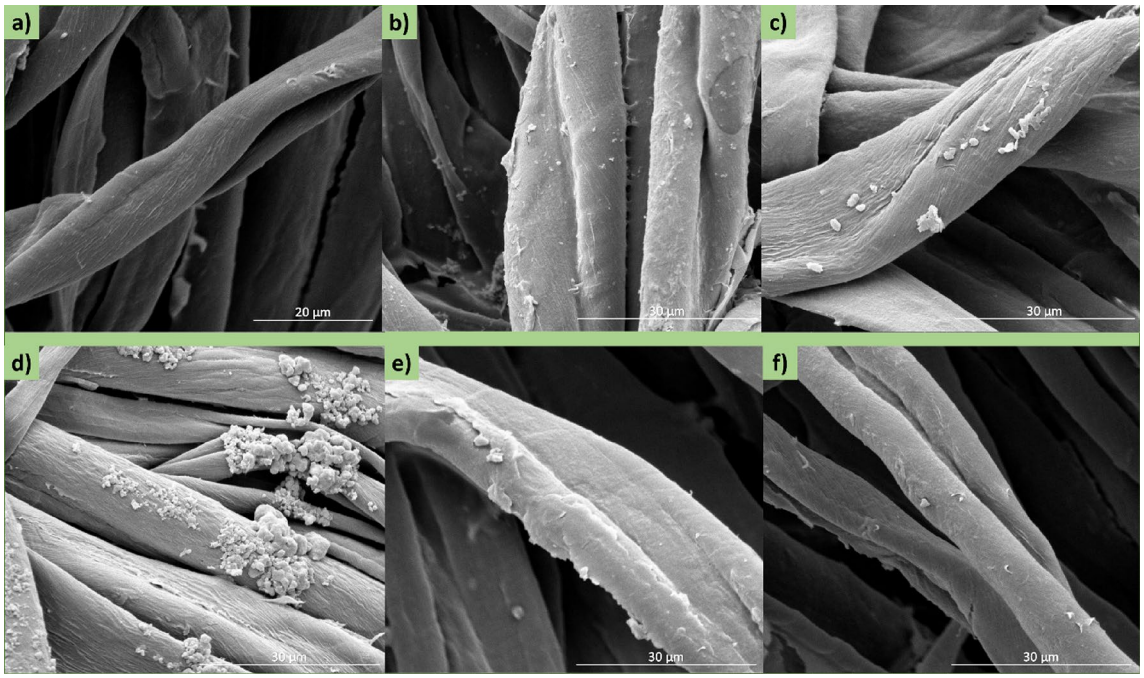

Fig. 2 SEM images for untreated and treated cotton fibers with zinc oxide (ZnO) and copper nitrate trihydrate by hydrothermal route. **a** Untreated cotton fiber (CF). CF treated with several concentrations of citric acid, corresponding in **b** 0, **c** 1, **d** 3, **e** 5, and **f** 10 g L^{-1}

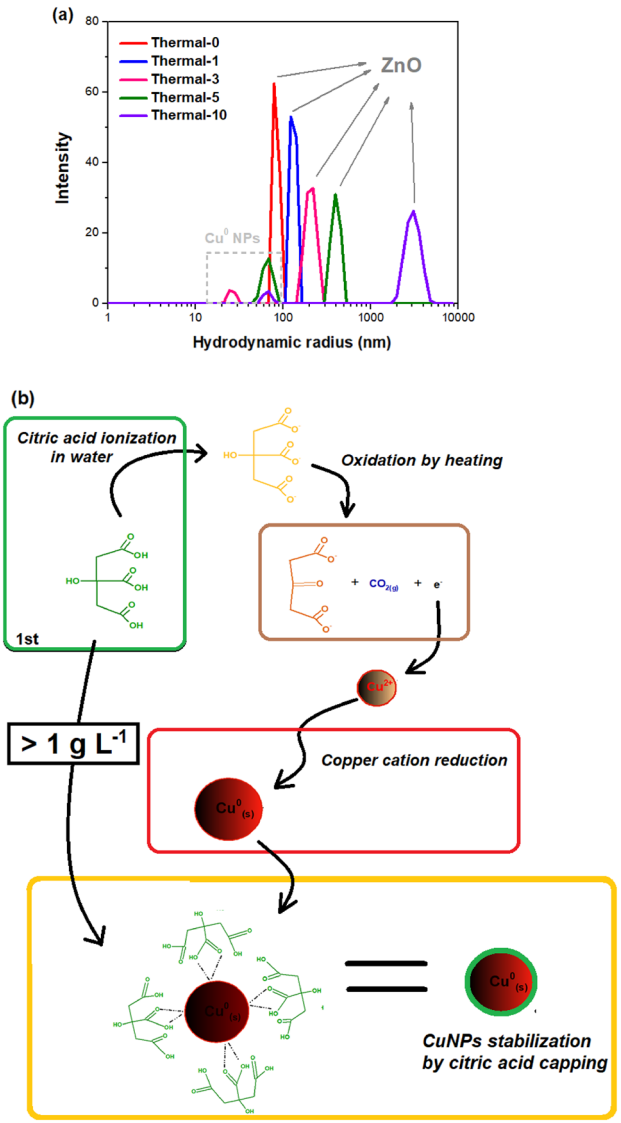

Fig. 3 **a** Hydrodynamic size of ZnO and Cu particles in the colloidal dispersion bath of cotton fibers after the hydrothermal procedure with several concentrations of citric acid (0, 1, 3, 5, and 10 g L^{-1}). **b** Illustration of the stages involving the formation of copper nanoparticles due to oxidation of citric acid molecules due to heating in the hydrothermal treatment

particles on the fiber's surface increased according to higher concentrations of reductant/binder agent. The adhesion of ZnO-NPs and Cu-NPs on the fiber's surface occurred intensively after the treatment with citric acid, as can be seen on the XPS spectra (Fig. 1S) and the atomic content evaluation (Fig. 2S) based on binding characteristics signals at 933 (Cu^0 $2p_{3/2}$), 952.5 (Cu^0 $2p_{1/2}$), 1020.7 (ZnO $2p_{3/2}$), and 1043.5 (ZnO $2p_{1/2}$) [42, 44–50]. Wu and co-workers [51] observed the same behavior caused by the addition of citric acid. They observed an increase of the Ag-NPs coating on the cotton fibers after treatment with citric acid [51].

Figure 3b illustrates the reaction steps involving reducing Cu^{2+} to Cu^0 due to the citric acid ionization, followed by oxidation that causes electrons liberation, reducing the copper cations. The hydrodynamic size distribution of the colloidal bath indicates that the increase of the citric acid content provokes agglomeration of ZnO-NPs that can be justified by condensation reactions of –COOH and –OH from citric acid and ZnO. Moreover, only above 1 g L^{-1} the citric acid can lead to the formation and stabilization of CuNPs in the colloidal bath, but this acid concentration is enough to cause the formation of copper nanoparticles on the cotton fibers' surface. Above 10 g L^{-1}, the formation of micrometric agglomerates of ZnO in the aqueous treatment bath is observed. Microparticles agglomeration on the coated fiber's surface was observed for the citric acid concentration of 3 g L^{-1}.

Another characteristic observed from higher citric acid concentrations for the thermal-X% samples was an apparent roughness of the cotton fiber. This phenomenon may be associated with a swelling and dissolution process of the amorphous cellulose on the cotton fiber's surface. Chen et al. [52] obtained the same morphology for functionalized cotton fabrics by combining polyvinylsilsesquioxane and nano-TiO_2. An apparent roughness was observed on the surfaces of the functionalized cotton fibers, and the higher apparent roughness was attributed to higher concentrations of binder and nanoparticles [52]. Noorian, Hemmatinejad & Navarro [53] attributed an increase in roughness of cellulose fibers on the cotton fabric due to the deposition of ZnO on the surface of treated cotton fibers.

3.2 FT-Raman

As shown in Fig. 3S, the cotton fibers display characteristic Raman shifts bands associated with cellulose molecular vibrations [54]: CCC and CCO ring deformation (339 and 384 cm^{-1}); CCC ring deformation (438 and 456 cm^{-1}); COC glycosidic linkage (518 cm^{-1}); CH skeletal rotating (900 cm^{-1}); COC in glycosidic linkages—symmetric and asymmetric stretching (1100 and 1150 cm^{-1}); CH_2 vibration (1328, 1373, and 1480 cm^{-1}); and CH stretching (2886 cm^{-1}). The cellulose crystallinity of the CF sample is 60% according to the ratio between the crystalline cellulose (1475 cm^{-1}) and its amorphous form (1450 cm^{-1}) [55].

The thermal treatment resulted in samples with a similar chemical structure of the CF sample, indicating cellulose's presence (Fig. 4a and b). The main changes were verified at 1472, 1418, 1339, and 340–330 cm^{-1}, all associated with cellulosic chain vibrations. However, it is not detected by FT-Raman ZnO-NPs that present fundamental phonon modes (Fig. 3S insert) at 333 cm^{-1} (zone boundary phonons $3E_2H$-E_2L), 350 cm^{-1} (E_2(High)), 386 cm^{-1} (E_2 (Low)), 438 cm^{-1} (A_1(TO)), 579 cm^{-1} (E_2(High)),

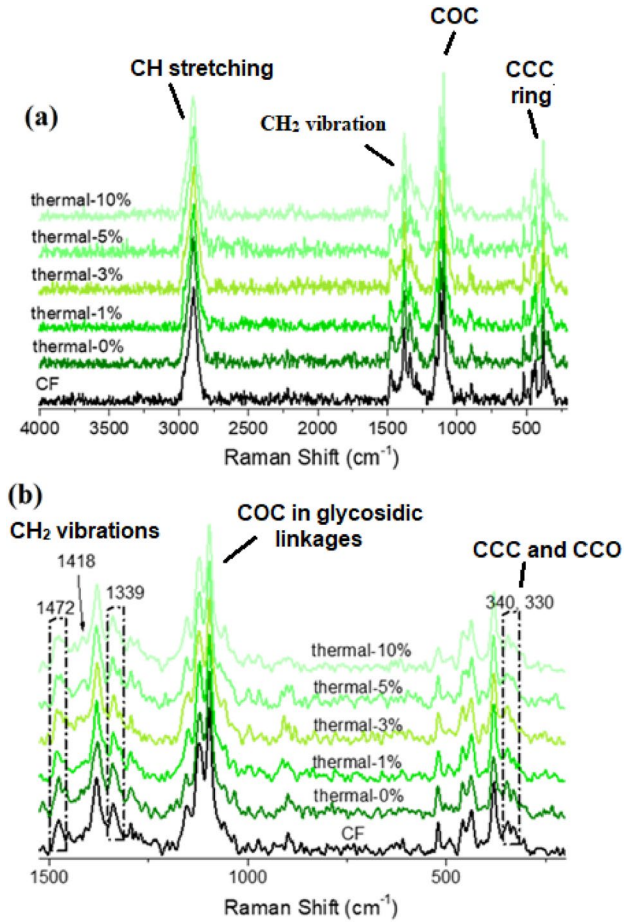

Fig. 4 FT-Raman spectra of thermal-treated samples on the Raman shift ranges: **a** 4000–200 cm^{-1}, and **b** 1500–200 cm^{-1}

604 cm^{-1} (TO + TA (M)), 627 cm^{-1} (E_1(LO)), 706 cm^{-1} (E_2(Low)) and 756 cm^{-1} (B_1(High)) [56, 57].

In the thermal treatment, cellulose fibers are expected to swell and facilitate ZnO and copper nanoparticles' diffusion through the thread attached to cotton fibers' surface. After drying, the excess water is removed by evaporation, and the particles are kept inside the thread. The thermal treatment for cotton fibers' crosslink with citric acid is commonly reported in the literature since the temperature favors this reaction [58]. In this case, the crosslink reactions could help the particles to stay inside the thread.

Using FT-Raman data, the crystallinity of thermal-0%, thermal -1%, thermal-3%, thermal-5%, and thermal-10% was 53.5%, 52.6%, 51.0%, 50.7%, and 50.6%, respectively. The crystallinity results were calculated by FT-Raman, which considers the cellulose structure, and presented a decreasing tendency with higher binding agent concentration. These observations arise from the treatment that promotes a disturbance of the crystalline structure caused by fiber swelling and thermal exposure. Additionally, the nanoparticles attached to the fibers' surface may impact the swelling and diffusion process.

3.3 X-Ray Diffractometry

Figure 5a presents the XRD patterns of the cotton fibers before and after functionalization. Amorphous cellulose phase and two monoclinic crystals from the cellulose polymorphism are identified [59–62]: cellulose I_β (x-ray diffraction signals at $2\theta = 14.7°$ (1 $\bar{1}$ 0), 16.5° (110), 22.5° (200), and 34.5° (004)) and cellulose II (x-ray diffraction signals at $2\theta = 12.4°$ (1 $\bar{1}$ 0), 20.2° (110), and 38.3° (301)). Other polymorphic forms of cellulose can be found in the cotton fibers, such as cellulose Iα, III_I, III_{II}, IV_I, and IV_{II} that can be interconverted by chemical routes [63].

It was not detected by XRD the presence of wurtzite ZnO-NPs (2θ signals at 34.5° (002), 36.5° (101), 47.7° (102), 56.9° (110), 62.7° (103), 66.4° (200), 67.8° (112), 69.3° (201), 72.7° (004) and 77.1° (202)) [64, 65] and Cu-NPs (2θ signals at 43.2°(111), 50.1° (200), and 74.1° (220)) [66, 67] on the functionalized cotton fibers. The shallow content (ppm) of copper ions and zinc oxide particles in the colloidal bath [8] and overlapping of X-ray signals from the NPs by the amorphous cellulose halo and other components in the CF (such as hemicellulose, lignin, and pectins) [68] can explain this absence of the x-ray diffraction from the crystal planes of the ZnO and copper nanoparticles in the XRD data from the functionalized cotton fibers.

As shown in Fig. 5b, the XRD crystallinity index (CI_{XRD}) for the CF sample equals 46.1% by Rietveld refinement. The hydrothermal treatment leads to a bit of increase in the CF's total crystallinity. Nam et al. [69] reported an amorphous fraction of 46% in bleached cotton fibers. However, the cellulose crystallinity index in vegetable sources depends on biological and environmental factors, including climatic conditions, soil composition, plant species, and fiber treatment. Moreover, the calculation method and the measurement technique (e.g., solid-state nuclear magnetic resonance or XRD) can lead to different crystallinity index values [70, 71]. The Rietveld method is suitable for detecting changes in the crystalline structure, obtaining X-ray peak profile parameters, and estimating the CI_{XRD} by fitting the whole diffraction pattern. However, it requires previous information about the unit cell, space group, and atomic coordinates [72].

The lattice parameters of cellulose in the natural fibers were determined by the Rietveld refinement (Fig. 4S) to get more information about the effect of these two parameters on the crystalline phases present in them. The XRD curves calculated by refinement present good agreement with the observed x-ray patterns, presenting goodness-of-fit ($1 < \chi^2 < 2$) that is considered an excellent reliability factor for refinement processes involving XRD experimental data of semicrystalline polymer systems [73–75].

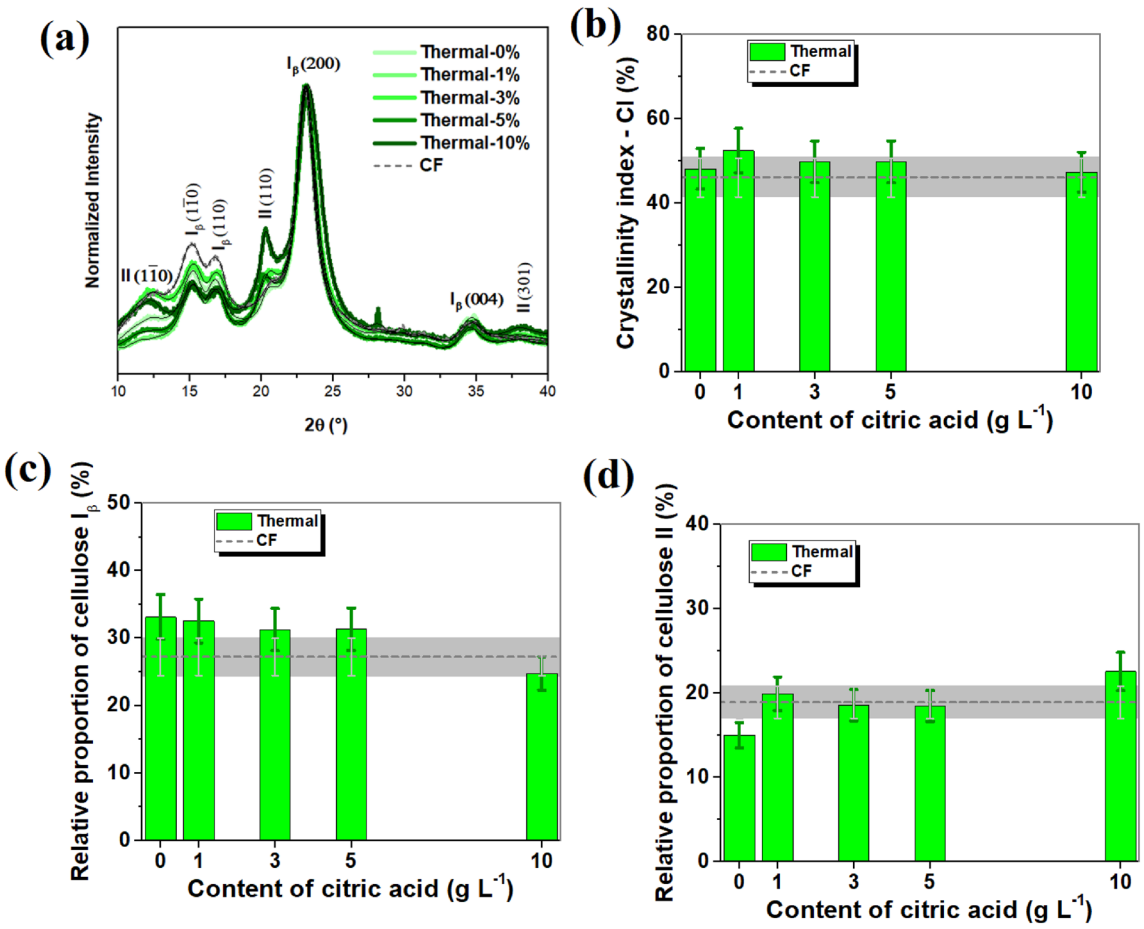

Fig. 5 X-ray diffractograms for the washed cotton fibers (CF) treated with zinc oxide, copper nitrate trihydrate, and several concentrations of citric acid (**a**). The X-ray diffractograms calculated by the Rietveld refinement are in continuous black lines. I_β and II denote two different monoclinic crystal systems of cellulose (**a**). The XRD crystallinity index (CI_{XRD}) (**b**), relative proportions of cellulose I_β (**c**) and II (**d**) calculated by Rietveld refinement

For CF sample, the unit cell dimensions calculated for cellulose I_β are $a=7.7$ Å, $b=8.2$ Å, $c=10.3$ Å, $\alpha=\beta=96.7°$, and $\gamma=96.5°$, while cellulose II unit cell presents $a=7.9$ Å, $b=9.1$ Å, $c=10.4$ Å, $\alpha=\beta=90°$, and $\gamma=118.0°$. These results indicate only a significant difference in the γ angle on the cellulose I_β unit cell according to the cellulose crystal data reported in the literature [61, 76]. Tukey's test results (Table 1S) show that citric acid content does have no significant effect over the lattice parameters of cellulose II and I_β crystals but modifies the relative proportion of cellulose I_β and the XRD crystallinity index (CI_{XRD}) significantly.

3.4 Wetness

The superficial modification of cotton fibers using different materials (e.g., dyes, pigments) and physical treatments (e.g., heating and ultrasound) can negatively and undesirably affect other functional properties of the cotton wipes. According to Fig. 6, the cotton fibers' wetness is reduced

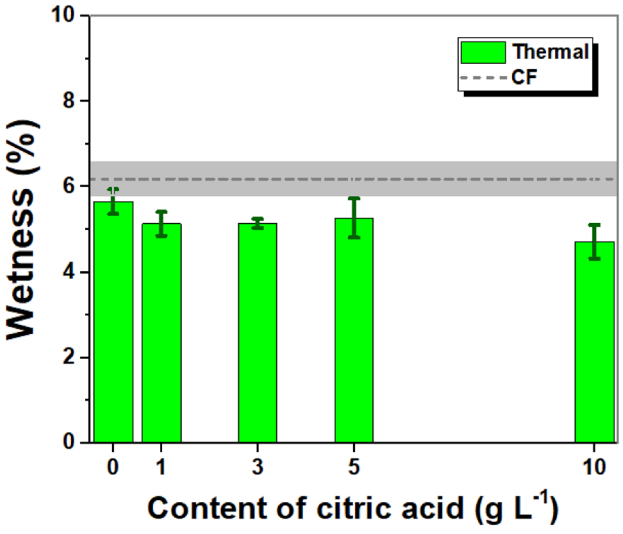

Fig. 6 Wetness for the cotton fiber (CF) treated with zinc oxide, copper nitrate trihydrate, and several concentrations of citric acid by hydrothermal route

with the increase of citric acid in the hydrothermal treatment. The wetness of the CF is 6.2 ± 0.4%. Tukey's test (Table 2S) confirms that the wetness of CF is significantly different from that observed for thermal-X% samples, but the humidity retention of the thermal-X% samples is similar among them. The ZnO and copper particles retained on the surface of the functionalized samples are responsible for their low capacity to retain moisture.

The high affinity between water and cellulose molecules is responsible for the moisture in natural fibers. However, the wetness combined with human body secretions can cause the proliferation and growth of pathogenic and odor-generating microorganisms in cotton textiles [9].

3.5 UV–Vis Spectroscopy

The transmittance in the visible electromagnetic spectrum of the samples is presented in Fig. 7. The wipe with pristine cotton fibers (CF) absorbs 95% of the electromagnetic radiation in the range of 500–800 nm. The fixation of copper and zinc oxide particles does not completely inhibit the passage of visible light by photon scattering and absorption due to empty spaces between the braided fibers in the cotton threads.

The wurtzite hexagonal ZnO-NPs present optical bandgap in the UV radiation region (< 400 nm) with a photo-physical bandgap higher than 3.2 eV, which can vary depending on the different levels of oxygen vacancies, particle format, and particle size distribution [77, 78]. Non-oxidized CuNPs in colloidal dispersions and cotton fiber absorb visible light (around 575 nm) due to the surface plasmon resonance [79, 80]. Nevertheless, the characteristic absorption bands of CuNPs and ZnO-NPs were not detected on the UV–Vis spectra. The low concentration of CuNPs on the surface of the CF modified with Cu^{2+} and ZnO with citric acid justifies this phenomenon [36].

According to the results obtained by UV–Vis spectroscopy (Fig. 7) and Tukey's test (Table 2S), both T(UVA) and T(UVB) of the CF are significantly reduced due to the treatment citric acid content applied during the treatment. This

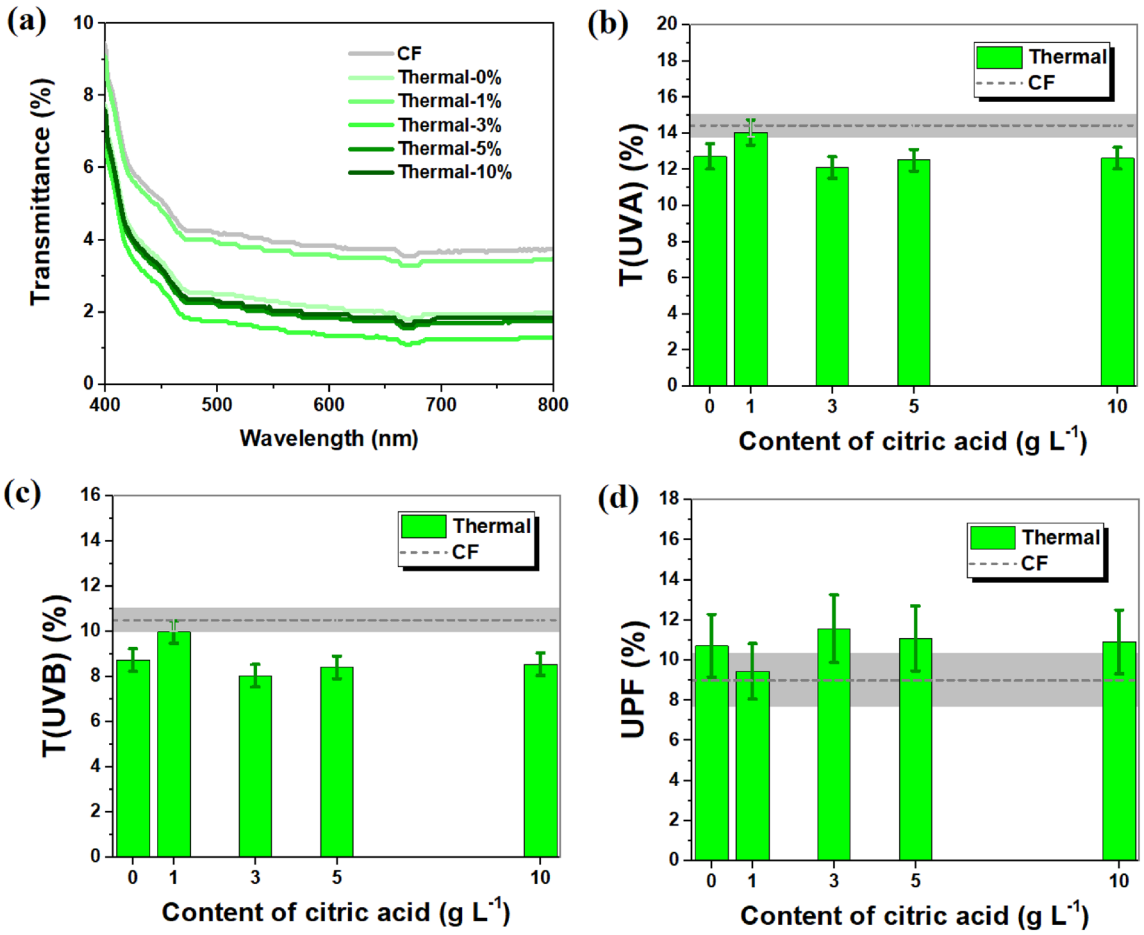

Fig. 7 UV–Vis spectra (**a**), T(UVA) (**b**), T(UVB) (**c**), and UPF (**d**) for the wipes with cotton fibers functionalized with copper and zinc oxide using several concentrations of citric acid

reduction in the UV transmission radiation of cotton textiles is indicative of increasing on the UV radiation scattering and absorption occasioned by the inorganic particles bonded on the cotton fibers [36], enhancing the UV protection capacity of cotton threads that has substantial importance to prevent severe dermatological complications and diseases caused by skin exposition to solar radiation [8].

The Ultraviolet Protection Factor (UPF) of the samples was conducted without prior drying, but Louris et al. [81] warn that the sample's humidity can affect the UV protection capacity of cotton fibers. The UPF of the CF is 8.9 ± 1.3%, being enhanced by the surface modification route. The most significant increase is observed for the thermal-3% sample, whose increase in the UPF reached 37.5%.

3.6 Mechanical Properties

The obtained stress–strain curves are presented in Fig. 5S, and Table 1 summarizes the mechanical results in terms of Young Modulus (E), tensile strength (σ), and elongation at break (ε) of the multifunctional cotton wipes. The samples with mechanical properties statistically similar, considering a 95% confidence level (Tukey's test), are indicated by similar letters. All samples presented statistically similar results for ε, indicating that the applied treatment and particle incorporation present a negligible effect over the elongation at break, which may be related to multilayer and braided structure that restricts the cotton wipe deformation [82].

Evaluating the Young Modulus is observed a substantial reduction from 205 ± 10 MPa to values lower than 165 MPa when more than 3 g L^{-1} of citric acid was applied during the treatment. The tensile strength is also significantly reduced at this condition of citric acid content, presenting a reduction that can exceed 50%. This loss of mechanical properties can be justified by the increase of defects in the cotton fibers and reduction of crystalline cellulose, which were observed by SEM and FT-Raman results due to the combined action of citric acid and temperature.

Table 1 Mechanical properties of developed wipes with cotton fibers

Sample	Young modulus (MPa)	Tensile strength (MPa)	Elongation (%)
CF	205 ± 10^{a}	14.6 ± 1.4^{a}	8.0 ± 0.5^{a}
Thermal-0	203 ± 8^{a}	$13.2 \pm 1.7^{a,b}$	8.0 ± 0.2^{a}
Thermal-1	208 ± 15^{a}	$9.6 \pm 2.0^{a,b,c}$	7.9 ± 0.2^{a}
Thermal-3	138 ± 6^{b}	$8.0 \pm 0.2^{b,c}$	8.2 ± 0.7^{a}
Thermal-5	153 ± 9^{b}	6.9 ± 1.6^{c}	7.3 ± 0.5^{a}
Thermal-10	160 ± 2^{b}	$7.8 \pm 0.4^{b,c}$	7.9 ± 0.1^{a}

Young modulus (E), tensile strength (σ), and elongation at break (ε)

*The values are presented as mean ± standard deviation

**Samples with different letters in the same column are statistically different, considering a confidence level of 95%. The samples were compared in three different groups

3.7 Colorimetry

The color parameters L (brightness), a* (green–red), b* (blue–yellow), and ΔE (the difference between the cotton wipe's colors before and after the superficial treatments) are represented in Table 2 and Fig. 6S–7S. Only the thermal-0% sample has a significantly lower ΔE and WI value than that for CF, suggesting a reduction of whiteness associated with the significant decrease of a* (green–red ratio) due to the presence of Cu^{2+} cations on the cotton wipe. These cations provoke the greening of the cotton fibers, as can be identified in Fig. 6S. ANOVA analysis followed by Tukey's test indicated that all cotton wipes treated with citric acid have similar color parameters.

3.8 Antimicrobial Activity

The inhibition halos in the agar nutrient medium due to the antimicrobial activity of the natural wipes against *E. coli* are shown in Fig. 8a and b. CF does not display bactericidal ability over *E. coli* colonies since it is not observed the formation of an inhibition halo on the Petri dishes after incubation of 48 h with or without illumination. All functionalized wipes do not display antimicrobial activity in darkness against *E. coli* in agar nutrient tests. Among the multifunctional cotton wipes under agar diffusion tests under illumination, it was observed that the thermal-0% and thermal-10% samples present antimicrobial activity, showing inhibition halos equal to 21 mm and 16 mm, respectively.

The higher antimicrobial performance of thermal-0% in diffusion test can be associated with the 3.1% atomic

Table 2 The surface color of wipes with pristine and surface-treated fibers

Samples	L*	a*	b*	ΔE	WI
CF[a]	88.3 ± 0.5	0.7 ± 0.1	8.7 ± 0.1	88.8 ± 0.2	85.4 ± 0.4
Thermal-0%[b]	83.4 ± 0.3	− 4.3 ± 0.5	9.4 ± 0.6	84.1 ± 0.2	80.5 ± 0.5
Thermal-1%[a,c]	88.8 ± 0.5	0.4 ± 0.3	8.5 ± 0.4	89.2 ± 0.1	85.9 ± 0.3
Thermal-3%[a,c]	89.1 ± 0.2	0.3 ± 0.2	8.3 ± 0.3	89.5 ± 0.1	86.4 ± 0.5
Thermal-5%[c]	89.4 ± 0.2	0.4 ± 0.2	8.3 ± 0.3	89.8 ± 0.1	86.5 ± 0.4
Thermal-10%[c]	89.6 ± 0.1	0.4 ± 0.1	8.3 ± 0.2	90.0 ± 0.1	86.8 ± 0.2

*The values are presented as mean ± standard deviation

**Samples with different letters are statistically different considering a confidence level of 95%. The samples were compared in three different groups

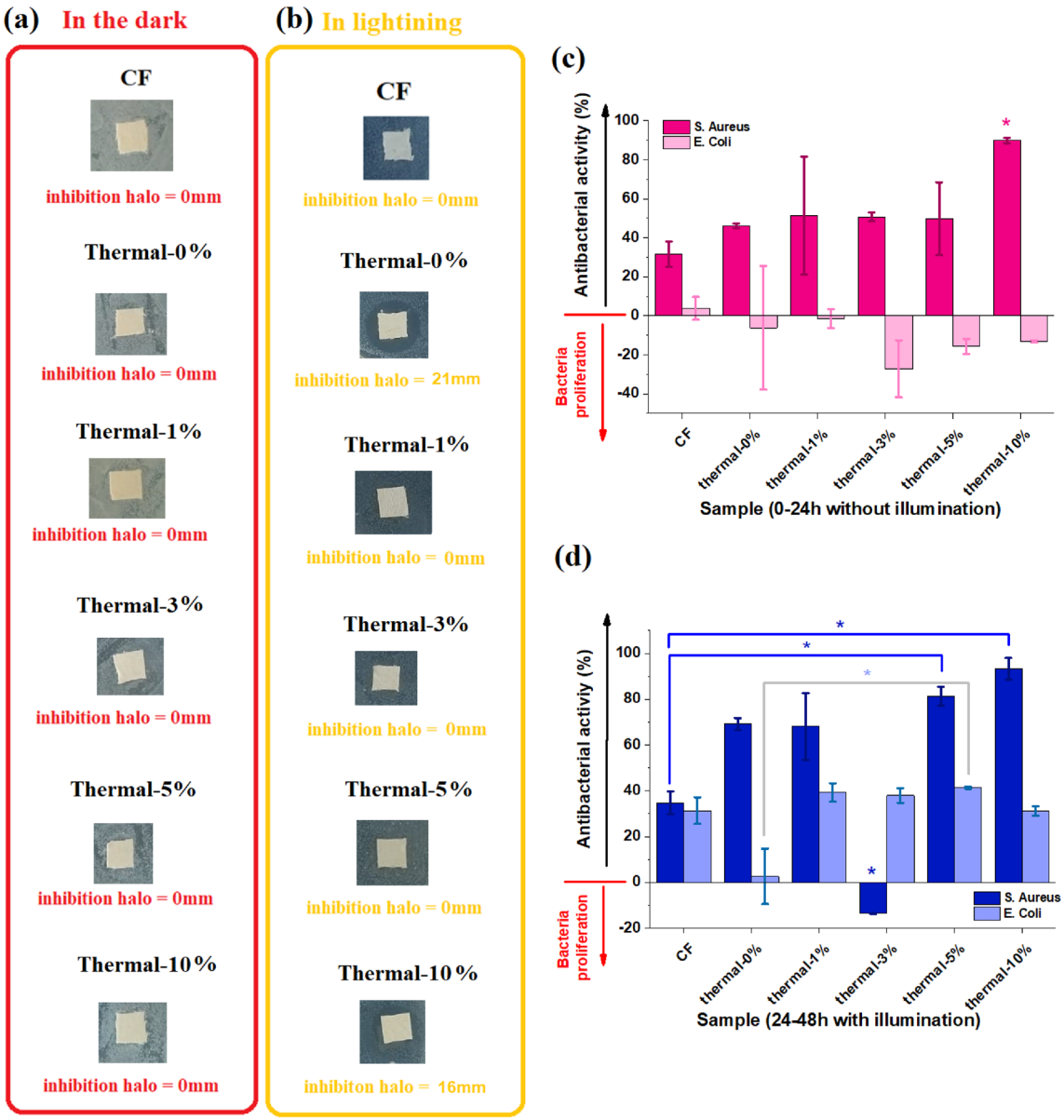

Fig. 8 Antimicrobial activity of the wipes with natural fibers treated with zinc oxide, copper nitrate trihydrate, and several concentrations of citric acid: **a** agar diffusion in darkness, **b** agar diffusion under lightning, **c** liquid growth inhibition test in darkness, and **d** liquid growth inhibition test under lightning. *Samples are statistically different, considering a confidence level of 95%

content of Cu^{2+} on the surface of the functionalized cotton wipes from XPS data (Fig. 2S), combined with a low atomic concentration for ZnO (0.01%). These copper ions are capable of generating active oxygen species (ROS) ($\cdot O_2^-$, H_2O_2, $^1O_2$, and $\cdot OH$) that cause oxidative stress of the bacterial cells (cell membrane damages, oxidation and cleavage of proteins, lipids, DNA, and RNA molecules) and are harmful against Gram-negative bacterial strains by non-oxidative mechanisms (irreversible damages to the cell wall via metal–biomolecules chemical interactions) [83–86].

The antimicrobial performance of the thermal-10% suggests that the wipes hybrid treated with ZnO/Cu^0 only show significative bactericidal effects against *E. coli* when the atomic content of ZnO and Cu^0 on the surface of cotton fibers is higher than 0.05% (Fig. 2S), in an atomic proportion of 1:1. ZnO and Cu^0 also cause oxidative stress by ROS, as Cu^{2+} cations, of the bacteria cells via photocatalytic mechanisms that depend on the optical bandgap, material defects, nanoparticle format and dimensions, and electronic levels.

The antibacterial activity in Fig. 8c obtained by liquid growth inhibition tests corroborates that the functionalized

cotton wipes do not show bactericidal activity against *E. coli* without illumination but present activity against *S. aureus*. The functionalization system ZnO/Cu^0 seems to be more effective against *S. aureus* than ZnO/Cu^{2+} systems in aqueous media, reaching an antimicrobial activity superior to 80% for the thermal-10% sample. The standard error of the measurements for the thermal-1% sample can be associated with the lowest Cu^0 content observed for thermal-1% (XPS data) that must cause a non-uniform coating of the fibers of the bacterial test specimens.

Under lighting (Fig. 8d), CF presents inhibition against *E. coli* and *S. aureus*, probably due to the formation of charged cellulose by ionization of acidic groups present on the cotton fibers (after conventional bleaching treatment) under electromagnetic irradiation that can cause bacteria membrane rupture [87, 88]. According to the liquid growth inhibition tests, the Cu^{+2}/ZnO functionalization does not display an antimicrobial effect on this bacteria under the liquid growth test conditions even when it is used illumination in the region of the visible electromagnetic spectrum corresponding to the blue color. The hydrothermal procedure possibly promotes a fiber's surface cleaning that removes any residual groups responsible for the inhibition observed for CF. However, with the Cu^0/ZnO surface functionalization using citric acid, an improvement in the antimicrobial activity of cotton fibers against *E. coli* was observed. Therefore, these results demonstrate that the developed fibers present potential antimicrobial properties related to the surface functionalization of Cu^0/ZnO nanoparticles and that lightning exposure can potentialize these properties through ROS generation. Moreover, it shows the potential to expand the development of cotton fibers with self-disinfecting properties by lightning exposure using a low-cost and feasible surface functionalization procedure.

4 Conclusions

Multifunctional wipes based on cotton fibers modified with hybrid ZnO/Cu^{2+} and ZnO/Cu^0 systems were successfully obtained by hydrothermal route with varied citric acid content. The increasing of citric acid concentration causes: increase of Cu-NPs hydrodynamic radius, agglomeration of ZnO-NPs, improvement of atomic content of ZnO and Cu^0 on the cotton fibers' surface, reduction of the cellulose crystallinity index (calculated by FT-Raman data), alterations in the relative proportion of cellulose I_β.

The Young modulus (MPa) and tensile strength (MPa) of the cotton wipes are compromised when more than 1 g L^{-1} of citric acid is utilized, which acts as an eco-friendly reducing agent of copper ions to form *in-situ* Cu-NPs on the cotton fiber surface. *In situ* synthesis of CuNPs and fixation ZnO-NPs reduce the wetness and improve the Ultraviolet Protection Factor (UPF), which is suitable to avoid the pathogenic microorganisms' proliferation and guarantee UV blocking multifunctional properties for cotton fibers. For the hydrothermal treatment, the addition of citric acid (1–10 g L^{-1}) leads to CF with similar colorimetric parameters for all concentrations, thus indicating that the agglomeration and content of nanoparticles present on the wipes do not influence its color difference (ΔE) and whiteness index (WI) values.

The ZnO/Cu^{2+} functionalized cotton fibers presented bactericidal activity against *E. coli* and S. *aureus* under lightning irradiation. The wipes with ZnO/Cu^0 functionalized cotton fibers show significant antimicrobial activity when the atomic content of ZnO and Cu^0 on the surface of cotton fibers achieve 0.05%, which was reached when it is applied 10 g L^{-1} of the citric acid content during the hydrothermal treatment. Both hybrid functionalizations based on copper and zinc oxide systems show potential applicability for the textile industry to fabricate antimicrobial intelligent clothes and personal protective equipment.

Supplementary Information The online version contains supplementary material available at https://doi.org/10.1007/s12221-023-00030-0.

Acknowledgements The authors thank the CAPES (Code 001), UFABC nº 48/2020—REIT (11.01), REVALORES, and Multiuser Central Facilities (UFABC) for the experimental support. This research was funded by Fundação de Amparo à Pesquisa do Estado de São Paulo (2019/16301-6), and Conselho Nacional de Desenvolvimento Científico e Tecnológico (305819/2017-8, CAPES-Pandemias 88881.504639/2020-01).

Data availability The data supporting the study's findings are available from the corresponding author upon reasonable request.

Declarations

Conflict of Interest The authors declare that they have no conflict of interest.

References

1. D.J. da Silva, H. Wiebeck, Current options for characterizing, sorting, and recycling polymeric waste. Prog. Rubber Plast. Recycl. Technol. **36**, 284–303 (2020). https://doi.org/10.1177/1477760620918603
2. J. Hu, ed., Active Coatings for Smart Textiles, Elsevier, Cambridge, UK, 2016. doi:https://doi.org/10.1016/C2014-0-00660-0.
3. M. Shahid, R. Adivarekar, eds., *Advances in Functional Finishing of Textiles*, Springer Singapore, Singapore, 2020: 1–388. https://doi.org/10.1007/978-981-15-3669-4.
4. P.J. Wakelyn, Cotton Fiber Chemistry and Technology, 1st ed. CRC Press, Boca Raton, 2006: pp. 1–176. https://doi.org/10.1201/9781420045888.
5. Y. Liu, Chemical composition and characterization of cotton fibers, in *Cotton fiber: physics chemistry and biology*. ed. by D.D. Fang (Springer International Publishing, Cham, 2018), pp.75–94. https://doi.org/10.1007/978-3-030-00871-0_4

6. D.D. Fang, *Cotton fiber: physics chemistry and biology* (Springer International Publishing, Cham, 2018), pp.151–178. https://doi.org/10.1007/978-3-030-00871-0
7. J.K. Patra, S. Gouda, Application of nanotechnology in food packaging: an overview. J. Eng. Technol. Res. **5**, 104–111 (2013). https://doi.org/10.5897/JETR2013-0309
8. S. Bhattacharjee, C.R. Macintyre, X. Wen, P. Bahl, U. Kumar, A.A. Chughtai, R. Joshi, Nanoparticles incorporated graphene-based durable cotton fabrics. Carbon N. Y. **166**, 148–163 (2020). https://doi.org/10.1016/j.carbon.2020.05.029
9. M.H. El-Rafie, H.B. Ahmed, M.K. Zahran, Characterization of nanosilver coated cotton fabrics and evaluation of its antibacterial efficacy. Carbohydr. Polym. **107**, 174–181 (2014). https://doi.org/10.1016/j.carbpol.2014.02.024
10. F.F. Yıldırım, O. Avinc, A. Yavas, G. Sevgisunar, Sustainable antifungal and antibacterial textiles using natural resources, in *Sustainability in the textile and apparel industries: sourcing natural raw materials*. ed. by S.S. Muthu, M.A. Gardetti (Springer Nature, Switzerland, 2020), pp.111–179
11. N. van Doremalen, T. Bushmaker, D.H. Morris, M.G. Holbrook, A. Gamble, B.N. Williamson, A. Tamin, J.L. Harcourt, N.J. Thornburg, S.I. Gerber, J.O. Lloyd-Smith, E. de Wit, V.J. Munster, Aerosol and surface stability of SARS-CoV-2 as compared with SARS-CoV-1. N. Engl. J. Med. **382**, 1564–1567 (2020). https://doi.org/10.1056/NEJMc2004973
12. A.G. Hassabo, M.E. El-Naggar, A.L. Mohamed, A.A. Hebeish, Development of multifunctional modified cotton fabric with tri-component nanoparticles of silver, copper and zinc oxide. Carbohydr. Polym. **210**, 144–156 (2019). https://doi.org/10.1016/j.carbpol.2019.01.066
13. M.S. Stan, I.C. Nica, M. Popa, M.C. Chifiriuc, O. Iordache, I. Dumitrescu, L. Diamandescu, A. Dinischiotu, Reduced graphene oxide/TiO2 nanocomposites coating of cotton fabrics with antibacterial and self-cleaning properties. J. Ind. Text. **49**, 277–293 (2019). https://doi.org/10.1177/1528083718779447
14. L.C. Giannossa, D. Longano, N. Ditaranto, M.A. Nitti, F. Paladini, M. Pollini, M. Rai, A. Sannino, A. Valentini, N. Cioffi, Metal nanoantimicrobials for textile applications. Nanotechnol. Rev. **2**, 307–331 (2013). https://doi.org/10.1515/ntrev-2013-0004
15. L.Y. Tan, L.T. Sin, S.T. Bee, C.T. Ratnam, K.K. Woo, T.-T. Tee, A.R. Rahmat, A review of antimicrobial fabric containing nanostructures metal-based compound. J. Vinyl Addit. Technol. **25**, E3–E27 (2019). https://doi.org/10.1002/vnl.21606
16. C. Balagna, S. Perero, E. Percivalle, E.V. Nepita, M. Ferraris, Virucidal effect against Coronavirus SARS-CoV-2 of a silver nanocluster/silica composite sputtered coating. Open Ceram. **1**, 100006 (2020). https://doi.org/10.1016/j.oceram.2020.100006
17. M.C. Sportelli, M. Izzi, E.A. Kukushkina, S.I. Hossain, R.A. Picca, N. Ditaranto, N. Cioffi, Can nanotechnology and materials science help the fight against SARS-CoV-2? Nanomaterials **10**, 802 (2020). https://doi.org/10.3390/nano10040802
18. K. Szabo, B.E. S, Removal of bacteria, viruses, and other microbial entities by means of nanoparticles, (Elsevier (2020) pp. 465–491.
19. V. Lysenko, V. Lozovski, M. Lokshyn, Y.V. Gomeniuk, A. Dorovskih, N. Rusinchuk, Y. Pankivska, O. Povnitsa, S. Zagorodnya, V. Tertykh, Y. Bolbukh, Nanoparticles as antiviral agents against adenoviruses. Adv. Nat. Sci. Nanosci. Nanotechnol. **9**, 025021 (2018). https://doi.org/10.1088/2043-6254/aac42a
20. U.S.E.P.A. EPA, List N: Disinfectants for Coronavirus (COVID-19), List N Disinfect. Coronavirus. 2:1–2 (2020). https://cfpub.epa.gov/wizards/disinfectants/.
21. M. Fiedot-Toboła, M. Ciesielska, I. Maliszewska, O. Rac-Rumijowska, P. Suchorska-Woźniak, H. Teterycz, M. Bryjak, Deposition of zinc oxide on different polymer textiles and their antibacterial properties. Materials (Basel). **11**, 707 (2018). https://doi.org/10.3390/ma11050707
22. Z.A. Raza, A. Rehman, M. Mohsin, S.Z. Bajwa, F. Anwar, A. Naeem, N. Ahmad, Development of antibacterial cellulosic fabric via clean impregnation of silver nanoparticles. J. Clean. Prod. **101**, 377–386 (2015). https://doi.org/10.1016/j.jclepro.2015.03.091
23. R. Krishnaveni, S. Thambidurai, Industrial method of cotton fabric finishing with chitosan–ZnO composite for anti-bacterial and thermal stability. Ind. Crops Prod. **47**, 160–167 (2013). https://doi.org/10.1016/j.indcrop.2013.03.007
24. Y. Shiraishi, H. Tanaka, H. Sakamoto, S. Ichikawa, T. Hirai, Photoreductive synthesis of monodispersed Au nanoparticles with citric acid as reductant and surface stabilizing reagent. RSC Adv. **7**, 6187–6192 (2017). https://doi.org/10.1039/C6RA27771C
25. S. Agnihotri, S. Mukherji, S. Mukherji, Size-controlled silver nanoparticles synthesized over the range 5–100 nm using the same protocol and their antibacterial efficacy. RSC Adv. **4**, 3974–3983 (2014). https://doi.org/10.1039/C3RA44507K
26. I. Perelshtein, G. Applerot, N. Perkas, E. Wehrschuetz-Sigl, A. Hasmann, G. Guebitz, A. Gedanken, CuO–cotton nanocomposite: Formation, morphology, and antibacterial activity. Surf. Coat. Technol. **204**, 54–57 (2009). https://doi.org/10.1016/j.surfcoat.2009.06.028
27. D. Breitwieser, M.M. Moghaddam, S. Spirk, M. Baghbanzadeh, T. Pivec, H. Fasl, V. Ribitsch, C.O. Kappe, In situ preparation of silver nanocomposites on cellulosic fibers–Microwave vs. conventional heating. Carbohydr. Polym. **94**, 677–686 (2013). https://doi.org/10.1016/j.carbpol.2013.01.077
28. A.M. Eremenko, I.S. Petrik, N.P. Smirnova, A.V. Rudenko, Y.S. Marikvas, Antibacterial and antimycotic activity of cotton fabrics, impregnated with silver and binary silver/copper nanoparticles. Nanoscale Res. Lett. **11**, 28 (2016). https://doi.org/10.1186/s11671-016-1240-0
29. S.B. Kashid, J.R. Lakkakula, D.S. Chauhan, R. Srivastava, R.W. Raut, Biocompatible antimicrobial cotton fibres for healthcare industries: a biogenic approach for synthesis of bio-organic-coated silver nanoparticles. IET Nanobiotechnol. **11**, 1046–1051 (2017). https://doi.org/10.1049/iet-nbt.2017.0077
30. J. Yang, H. Xu, L. Zhang, Y. Zhong, X. Sui, Z. Mao, Lasting superhydrophobicity and antibacterial activity of Cu nanoparticles immobilized on the surface of dopamine modified cotton fabrics. Surf. Coat. Technol. **309**, 149–154 (2017). https://doi.org/10.1016/j.surfcoat.2016.11.058
31. Z. Wu, W. Deng, J. Luo, D. Deng, Multifunctional nano-cellulose composite films with grape seed extracts and immobilized silver nanoparticles. Carbohydr. Polym. **205**, 447–455 (2019). https://doi.org/10.1016/j.carbpol.2018.10.060
32. Z. Jin, S. Wang, F. Yang, P. Dong, Z. Huang, X. Zhang, Y. Xiao, A two-step preparation method for nanocrystalline Ag-decorated cotton fabrics and their antibacterial assessment. J. Mater. Sci. **54**, 10447–10456 (2019). https://doi.org/10.1007/s10853-019-03637-y
33. S. Yokoyama, K. Motomiya, H. Takahashi, K. Tohji, Green synthesis of Cu micro/nanoparticles for low-resistivity Cu thin films using ascorbic acid in aqueous solution. J. Mater. Chem. C. **4**, 7494–7500 (2016). https://doi.org/10.1039/C6TC02280D
34. I. Marion, *Tobler-Rohr* (Woodhead Publishing, Cambridge, UK, Handbook of sustainable textile production, 2011)
35. N. Doebelin, R. Kleeberg, Profex: a graphical user interface for the Rietveld refinement program BGMN. J. Appl. Crystallogr. **48**, 1573–1580 (2015). https://doi.org/10.1107/S1600576715014685
36. H.E. Emam, T. Bechtold, Cotton fabrics with UV blocking properties through metal salts deposition. Appl. Surf. Sci. **357**, 1878–1889 (2015). https://doi.org/10.1016/j.apsusc.2015.09.095
37. X. Sun, J. Wang, H. Zhang, M. Dong, L. Li, P. Jia, T. Bu, X. Wang, L. Wang, Development of functional gelatin-based

composite films incorporating oil-in-water lavender essential oil nano-emulsions: Effects on physicochemical properties and cherry tomatoes preservation. LWT. **142**, 110987 (2021). https://doi.org/10.1016/j.lwt.2021.110987
38. V. Luccas, É.C. Bonomi, T.G. Kieckbusch, Caracterização comparativa entre chocolates ao leite formulados com gordura de leite anidra e com estearina de gordura de leite, Brazilian. J. Food Technol. **17**, 130–138 (2014). https://doi.org/10.1590/bjft.2014.020
39. R.R. Ferreira, A.G. Souza, D.S. Rosa, Essential oil-loaded nanocapsules and their application on PBAT biodegradable films. J. Mol. Liq. **337**, 116488 (2021). https://doi.org/10.1016/j.molliq.2021.116488
40. N.A. Ibrahim, B.M. Eid, E.A. El-Aziz, T.M. Abou Elmaaty, S.M. Ramadan, Multifunctional cellulose-containing fabrics using modified finishing formulations. RSC Adv. **7**, 33219–33230 (2017). https://doi.org/10.1039/C7RA05403C
41. M.E. Yazdanshenas, M. Shateri-Khalilabad, In situ synthesis of silver nanoparticles on alkali-treated cotton fabrics. J. Ind. Text. **42**, 459–474 (2013). https://doi.org/10.1177/1528083712444297
42. Z. Dan, Y. Yang, F. Qin, H. Wang, H. Chang, Facile fabrication of Cu2O nanobelts in ethanol on nanoporous cu and their photodegradation of methyl orange. Materials (Basel). **11**, 446 (2018). https://doi.org/10.3390/ma11030446
43. V. Sadanand, H. Tian, A.V. Rajulu, B. Satyanarayana, Antibacterial cotton fabric with in situ generated silver nanoparticles by one-step hydrothermal method. Int. J. Polym. Anal. Charact. **22**, 275–279 (2017). https://doi.org/10.1080/1023666X.2017.1287828
44. X. Wang, B. Zhang, W. Zhang, M. Yu, L. Cui, X. Cao, J. Liu, Super-light Cu@Ni nanowires/graphene oxide composites for significantly enhanced microwave absorption performance. Sci. Rep. **7**, 1584 (2017). https://doi.org/10.1038/s41598-017-01529-2
45. F. Liu, L. Csetenyi, G.M. Gadd, Amino acid secretion influences the size and composition of copper carbonate nanoparticles synthesized by ureolytic fungi. Appl. Microbiol. Biotechnol. **103**, 7217–7230 (2019). https://doi.org/10.1007/s00253-019-09961-2
46. L. Martin, H. Martinez, D. Poinot, B. Pecquenard, F. Le Cras, Comprehensive X-ray photoelectron spectroscopy study of the conversion reaction mechanism of CuO in lithiated thin film electrodes. J. Phys. Chem. C. **117**, 4421–4430 (2013). https://doi.org/10.1021/jp3119633
47. Y.-C. Liang, C.-C. Wang, Surface crystal feature-dependent photoactivity of ZnO–ZnS composite rods via hydrothermal sulfidation. RSC Adv. **8**, 5063–5070 (2018). https://doi.org/10.1039/C7RA13061A
48. M. Wang, L. Jiang, E.J. Kim, S.H. Hahn, Electronic structure and optical properties of Zn(OH) 2: LDA+U calculations and intense yellow luminescence. RSC Adv. **5**, 87496–87503 (2015). https://doi.org/10.1039/C5RA17024A
49. B. Rebhan, S. Tollabimazraehno, G. Hesser, V. Dragoi, Analytical methods used for low temperature Cu–Cu wafer bonding process evaluation. Microsyst. Technol. **21**, 1003–1013 (2015). https://doi.org/10.1007/s00542-015-2446-2
50. G. Yuan, J. Xiang, H. Jin, L. Wu, Y. Jin, Y. Zhao, Anchoring ZnO nanoparticles in nitrogen-doped graphene sheets as a high-performance anode material for lithium-ion batteries. Materials (Basel). **11**, 96 (2018). https://doi.org/10.3390/ma11010096
51. Y. Wu, Y. Yang, Z. Zhang, Z. Wang, Y. Zhao, L. Sun, Fabrication of cotton fabrics with durable antibacterial activities finishing by Ag nanoparticles. Text. Res. J. **89**, 867–880 (2019). https://doi.org/10.1177/0040517518758002
52. D. Chen, Z. Mai, X. Liu, D. Ye, H. Zhang, X. Yin, Y. Zhou, M. Liu, W. Xu, UV-blocking, superhydrophobic and robust cotton fabrics fabricated using polyvinylsilsesquioxane and nano-TiO2. Cellulose **25**, 3635–3647 (2018). https://doi.org/10.1007/s10570-018-1790-7
53. S.A. Noorian, N. Hemmatinejad, J.A.R. Navarro, Ligand modified cellulose fabrics as support of zinc oxide nanoparticles for UV protection and antimicrobial activities. Int. J. Biol. Macromol. **154**, 1215–1226 (2020). https://doi.org/10.1016/j.ijbiomac.2019.10.276
54. D. Puchowicz, P. Giesz, M. Kozanecki, M. Cieślak, Surface-enhanced Raman spectroscopy (SERS) in cotton fabrics analysis. Talanta **195**, 516–524 (2019). https://doi.org/10.1016/j.talanta.2018.11.059
55. K. Schenzel, S. Fischer, E. Brendler, New method for determining the degree of cellulose I crystallinity by means of FT Raman Spectroscopy. Cellulose **12**, 223–231 (2005). https://doi.org/10.1007/s10570-004-3885-6
56. R. Bomila, S. Suresh, S. Srinivasan, Synthesis, characterization and comparative studies of dual doped ZnO nanoparticles for photocatalytic applications. J. Mater. Sci. Mater. Electron. **30**, 582–592 (2019). https://doi.org/10.1007/s10854-018-0324-2
57. N. Senthilkumar, M. Ganapathy, A. Arulraj, M. Meena, M. Vimalan, I. Vetha Potheher, Two step synthesis of ZnO/Ag and ZnO/Au core/shell nanocomposites: Structural, optical and electrical property analysis. J. Alloys Compd. **750**, 171–181 (2018). https://doi.org/10.1016/j.jallcom.2018.03.348
58. A. Haji, S.M. Bidoki, F. Gholami, Isotherm and kinetic studies in dyeing of citric acid-crosslinked cotton with cationic natural dye. Fibers Polym. **21**, 2547–2555 (2020). https://doi.org/10.1007/s12221-020-1053-8
59. C. Fethiza Tedjani, O. Ben Mya, A. Rebiai, Isolation and characterization of cellulose from date palm tree spathe sheath. Sustain. Chem. Pharm. **17**, 100307 (2020). https://doi.org/10.1016/j.scp.2020.100307
60. C. Orrabalis, D. Rodríguez, L.G. Pampillo, C. Londoño-Calderón, M. Trinidad, R. Martínez-García, Characterization of nanocellulose obtained from *Cereus Forbesii* (a South American cactus). Mater. Res. **22**, 1–10 (2019). https://doi.org/10.1590/1980-5373-mr-2019-0243
61. K. Kafle, K. Greeson, C. Lee, S.H. Kim, Cellulose polymorphs and physical properties of cotton fabrics processed with commercial textile mills for mercerization and liquid ammonia treatments. Text. Res. J. **84**, 1692–1699 (2014). https://doi.org/10.1177/0040517514527379
62. D.J. de Silva, M.L.O. D'almeida, Nanocristais de celulose. O Pap. **70**, 34–52 (2009)
63. S. Rongpipi, D. Ye, E.D. Gomez, E.W. Gomez, Progress and opportunities in the characterization of cellulose – an important regulator of cell wall growth and mechanics, front. Plant Sci. **9**, 1–28 (2019). https://doi.org/10.3389/fpls.2018.01894
64. P.M. Perillo, M.N. Atia, D.F. Rodríguez, Studies on the growth control of ZnO nanostructures synthesized by the chemical method. Matéria (Rio Janeiro) (2018). https://doi.org/10.1590/s1517-707620180002.0467
65. M. Seray, A. Skender, A.S. Hadj-Hamou, Kinetics and mechanisms of Zn2+ release from antimicrobial food packaging based on poly (butylene adipate-co-terephthalate) and zinc oxide nanoparticles. Polym. Bull. (2020). https://doi.org/10.1007/s00289-020-03145-z
66. N. Sreeju, A. Rufus, D. Philip, Microwave-assisted rapid synthesis of copper nanoparticles with exceptional stability and their multifaceted applications. J. Mol. Liq. **221**, 1008–1021 (2016). https://doi.org/10.1016/j.molliq.2016.06.080
67. J.J. Ahire, M. Hattingh, D.P. Neveling, L.M.T. Dicks, Copper-containing anti-biofilm nanofiber scaffolds as a wound dressing material. PLoS ONE **11**, e0152755 (2016). https://doi.org/10.1371/journal.pone.0152755

68. A. El Oudiani, Y. Chaabouni, S. Msahli, F. Sakli, Crystal transition from cellulose I to cellulose II in NaOH treated Agave americana L. fibre. Carbohydr. Polym. **86**, 1221–1229 (2011). https://doi.org/10.1016/j.carbpol.2011.06.037
69. S. Nam, A.D. French, B.D. Condon, M. Concha, Segal crystallinity index revisited by the simulation of X-ray diffraction patterns of cotton cellulose Iβ and cellulose II. Carbohydr. Polym. **135**, 1–9 (2016). https://doi.org/10.1016/j.carbpol.2015.08.035
70. P. Ahvenainen, I. Kontro, K. Svedström, Comparison of sample crystallinity determination methods by X-ray diffraction for challenging cellulose I materials. Cellulose **23**, 1073–1086 (2016). https://doi.org/10.1007/s10570-016-0881-6
71. S. Park, J.O. Baker, M.E. Himmel, P.A. Parilla, D.K. Johnson, Cellulose crystallinity index: measurement techniques and their impact on interpreting cellulase performance. Biotechnol. Biofuels. **3**, 10 (2010). https://doi.org/10.1186/1754-6834-3-10
72. A. Thygesen, J. Oddershede, H. Lilholt, A.B. Thomsen, K. Ståhl, On the determination of crystallinity and cellulose content in plant fibres. Cellulose **12**, 563–576 (2005). https://doi.org/10.1007/s10570-005-9001-8
73. B.H. Toby, R factors in Rietveld analysis: How good is good enough? Powder Diffr. **21**, 67–70 (2006). https://doi.org/10.1154/1.2179804
74. M. Tsubota, J. Kitagawa, A necessary criterion for obtaining accurate lattice parameters by Rietveld method. Sci. Rep. **7**, 15381 (2017). https://doi.org/10.1038/s41598-017-15766-y
75. A. Lobo-Guerrero, X-ray analysis and Rietveld refinement of polyvinyl alcohol. Mater. Lett. **265**, 127434 (2020). https://doi.org/10.1016/j.matlet.2020.127434
76. A.D. French, Idealized powder diffraction patterns for cellulose polymorphs. Cellulose **21**, 885–896 (2014). https://doi.org/10.1007/s10570-013-0030-4
77. J. Estrada-Urbina, A. Cruz-Alonso, M. Santander-González, A. Méndez-Albores, A. Vázquez-Durán, Nanoscale zinc oxide particles for improving the physiological and sanitary quality of a mexican landrace of red maize. Nanomaterials **8**, 247 (2018). https://doi.org/10.3390/nano8040247
78. J.-H. Zhao, C.-J. Liu, Z.-H. Lv, Photoluminescence of ZnO nanoparticles and nanorods. Optik (Stuttg). **127**, 1421–1423 (2016). https://doi.org/10.1016/j.ijleo.2015.11.018
79. J. Ramyadevi, K. Jeyasubramanian, A. Marikani, G. Rajakumar, A.A. Rahuman, T. Santhoshkumar, A.V. Kirthi, C. Jayaseelan, S. Marimuthu, Copper nanoparticles synthesized by polyol process used to control hematophagous parasites. Parasitol. Res. **109**, 1403–1415 (2011). https://doi.org/10.1007/s00436-011-2387-3
80. G. Mary, S.K. Bajpai, N. Chand, Copper (II) ions and copper nanoparticles-loaded chemically modified cotton cellulose fibers with fair antibacterial properties. J. Appl. Polym. Sci. **113**, 757–766 (2009). https://doi.org/10.1002/app.29890
81. E. Louris, E. Sfiroera, G. Priniotakis, R. Makris, H. Siemos, C. Efthymiou, M.N. Assimakopoulos, Evaluating the ultraviolet protection factor (UPF) of various knit fabric structures. IOP Conf. Ser. Mater. Sci. Eng. **459**, 012051 (2018). https://doi.org/10.1088/1757-899X/459/1/012051
82. Y.R. Zhang, J.T. Chen, B. Hao, R. Wang, P.C. Ma, Preparation of cellulose-coated cotton fabric and its application for the separation of emulsified oil in water. Carbohydr. Polym. **240**, 116318 (2020). https://doi.org/10.1016/j.carbpol.2020.116318
83. K. Szabo, B.E. S, D.C. Vodnar, L. Mitrea, L.F. Călinoiu, K. Szabo, B.E. Ştefănescu, Removal of bacteria, viruses, and other microbial entities by means of nanoparticles In: Advanced Nanostructures for Environmental Health, Elsevier, 2020: pp. 465–491. https://doi.org/10.1016/B978-0-12-815882-1.00011-2
84. M.P. Cervantes-Cervantes, J.V. Calderón-Salinas, A. Albores, J.L. Muñoz-Sánchez, Copper increases the damage to dna and proteins caused by reactive oxygen species. Biol. Trace Elem. Res. **103**, 229–248 (2005). https://doi.org/10.1385/BTER:103:3:229
85. K.V.T. Nguyen, F.S. Ameer, J.N. Anker, J.L. Brumaghim, H.C. Minh, Reactive oxygen species generation by copper(II) oxide nanoparticles determined by DNA damage assays and EPR spectroscopy. Nanotoxicology **11**, 278–288 (2017). https://doi.org/10.1080/17435390.2017.1293750.Reactive
86. J. Liu, J. Wang, S. Lee, R. Wen, Copper-caused oxidative stress triggers the activation of antioxidant enzymes via ZmMPK3 in maize leaves. PLoS ONE **13**, e0203612 (2018). https://doi.org/10.1371/journal.pone.0203612
87. M.M. Mahat, A.S.M. Sabere, J. Azizi, N.A.N. Amdan, Potential Applications of conducting polymers to reduce secondary bacterial infections among COVID-19 patients: a review. Emerg. Mater. **4**, 279–292 (2021). https://doi.org/10.1007/s42247-021-00188-4
88. J. BeMiller, R. Whistler, eds., Starch, 3rd ed., Elsevier, New York, NY, 2009. doi:https://doi.org/10.1016/S1082-0132(08)X0009-3.